Heliyon 10 (2024) e35377

Contents lists available at ScienceDirect

Heliyon

journal homepage: www.cell.com/heliyon

Research article

Analysis of influence mechanism of CO_2-water coupling fracturing sandstone

Hongjian Li [a,b,*], Guangzhe Deng [a,b]

[a] Key Laboratory of Western Mine Exploitation and Hazard Prevention Ministry of Education, Xi'an University of Science and Technology, Xi'an, 710054, Shanxi Province, China
[b] School of Energy Engineering, Xi'an University of Science and Technology, Xi'an, 710054, Shanxi Province, China

ARTICLE INFO

Keywords:
CO_2-Water-rock coupling
Thick hard sandstone gangue layer
Pore structure
Crushing mechanism

ABSTRACT

The existence of hard rock layers has a serious impact on coal seam mining, in order to explore the acidification and crushing mechanism of hard sandstone rock layers, this paper adopts the self-developed CO_2-water-rock coupling test device to carry out the testing of mechanical properties and internal structural characteristics of rock samples before and after the coupling action of the three sandstones, and analyzes the influencing factors of sandstone CO_2 coupling crushing. The study shows that: the lower the temperature of CO_2-water-rock coupling, the higher the pore pressure, the higher the volume fraction of CO_2 in the coupling fracturing fluid, and the longer the coupling time, the greater the decrease in the mechanical strength of the rock samples, and the more complicated the splitting damage pattern is, and the CO_2-water-rock coupling makes the pore and fracture volume fraction and fractal dimension of three kinds of sandstone samples increase to varying degrees, whereas the volume fraction of minerals and the fractal dimension decrease, and the CO_2-water-rock coupling results in a decrease in the volume fraction of minerals and fractal dimension, and a decrease in the volume fraction of minerals and fractal dimension. The pore volume fraction and fractal dimension of the three sandstone samples increased to different degrees, while the mineral volume fraction and fractal dimension decreased, and the pore volume fraction and fractal dimension of the three sandstone samples decreased. The damage pattern of sandstone samples after coupling is affected by both chemical and mechanical damages. When using coupling fracturing fluid with 8 % CO_2, the degree of mineral dissolution and dissolution is the largest, and the dissolution effect is larger than the precipitation effect, which has the most significant effect on the morphology type and connectivity of microscopic pore cracks, and the study in this paper has certain theoretical and practical value for the chemical softening of sandstone.

1. Introduction

Global warming is one of the most serious challenges facing the world today. It has a huge impact and threat on human society and natural ecosystems [1–6]. The Paris Agreement requires countries to achieve a balance between greenhouse gas emissions and absorption in the second half of this century, that is, to achieve carbon neutrality. In order to cope with global warming and achieve the

* Corresponding author. Key Laboratory of Western Mine Exploitation and Hazard Prevention Ministry of Education, Xi'an University of Science and Technology, Xi'an, 710054, Shanxi Province, China.
E-mail address: lhj164343@163.com (H. Li).

https://doi.org/10.1016/j.heliyon.2024.e35377
Received 26 January 2024; Received in revised form 25 July 2024; Accepted 26 July 2024
Available online 27 July 2024

goal of carbon neutrality, governments and international organizations have taken a series of measures, including reducing greenhouse gas emissions, improving energy efficiency, developing renewable energy, strengthening climate adaptability, promoting green and low-carbon development, adopting carbon capture and storage technologies and energy utilization of carbon dioxide [7–12].

In recent years, CO_2-water-rock coupling fracturing technology has received extensive attention from domestic and foreign experts in the coal industry because of its many advantages, such as increasing coal production, no pollution of reservoirs, saving water resources, and effectively burying CO_2, etc., and CO_2 phase-change fracturing has been expected in the field of anhydrous fracturing technology [13–17]. In order to investigate the mechanism of CO_2-water-rock coupling action and improve the level of rock fracturing and CO_2 utilization efficiency, scholars at home and abroad have carried out a large number of experimental studies, simulations and field practices, basically determining the damage damage law of the rock body when the CO_2 fracturing fluid is injected into the conventional rock formations [18–23], and grasping to a certain extent the properties of the rock body itself (mineral composition [24], mechanical strength [25] pore structure [26], permeability, water content [27], etc.), the properties of CO_2 fracturing fluid [28], phase state [29], salt concentration [30], and the coupling conditions (temperature, pressure [31,32], time of action [33], etc.) on the damage of the rock, which effectively improves the effect of coupled fracturing. However, at present, the main target rock of CO_2-water-rock coupling is shale, and there are fewer studies on CO_2-water-rock coupling crushing mechanism in coal bed hard sandstone, and the number of cycles of coupling action is often ignored, the influence of the softening effect, the pore and fracture structure of the rock layer of the CO_2-water-rock coupling action, and the mechanism of mechanical and chemical composite damage is still unclear and its influencing factors have not been fully quantified [34–38].

Therefore, to address the problem of hard rock fragmentation, this paper combines the principle of hydraulic fracturing with the technical advantages of CO_2 fracturing, with the goal of revealing the softening mechanism of CO_2-water-rock coupled fracturing of hard sandstone at the working face, analyzing the influencing factors of sandstone softness and permeability through the physico-chemical modification of sandstone under the action of CO_2-water-rock coupling, and researching the intrinsic relationship between the fracturing pore cleavage dissolution and solvation and the destructive deformation of the sandstone.

2. Experimental materials and methods

2.1. Rock sample collection and fracturing fluid preparation instructions

In this paper, the gangue samples were taken from the 112201 comprehensive mining face of Xiaobaodang coal mine in the Jurassic of northern Shaanxi Province, China. On-site geological exploration shows that, as shown in Fig. 1a, there is a continuous distribution of hard sandstone rock strata along the strike of the coal beds in the range of 100~560m, which runs through the whole length of the face, with the lithology dominated by siltstone and fine-grained sandstone, and a small amount of medium-grained sandstone and coarse-grained sandstone, which shows excellent solidity properties, and Fig. 1b shows some of the original samples of the three sandstone rocks during the experimental sampling of the samples. Fig. 1b shows some of the original samples of the three sandstones during our experimental sampling.

The samples used for all experiments and tests in this paper are sandstones with lithologies of siltstone, fine-grained sandstone, and coarse-grained sandstone, respectively. During sampling, columnar rock samples with a diameter of 50 ± 0.1 mm were drilled from the downhole cores, and then the end faces of the processed samples were polished and made to be parallel to the cylindrical surfaces (Fig. 2) in order to meet the requirements of the subsequent tests.

The key to CO_2-coupled fracturing fluid preparation is the preferred selection of surfactant and the determination of CO_2 mass fraction, and the compound surfactant is selected for the physical and mechanical characteristics of the hard sandstone layer to be fractured and softened. According to the relevant research results of the team's coal rock softening active fracturing materials [39], in

Fig. 1. Experimental samples (a is empirical evidence of sandstone rock exposed in the coal wall of the working face, b is partial sandstone sampling).

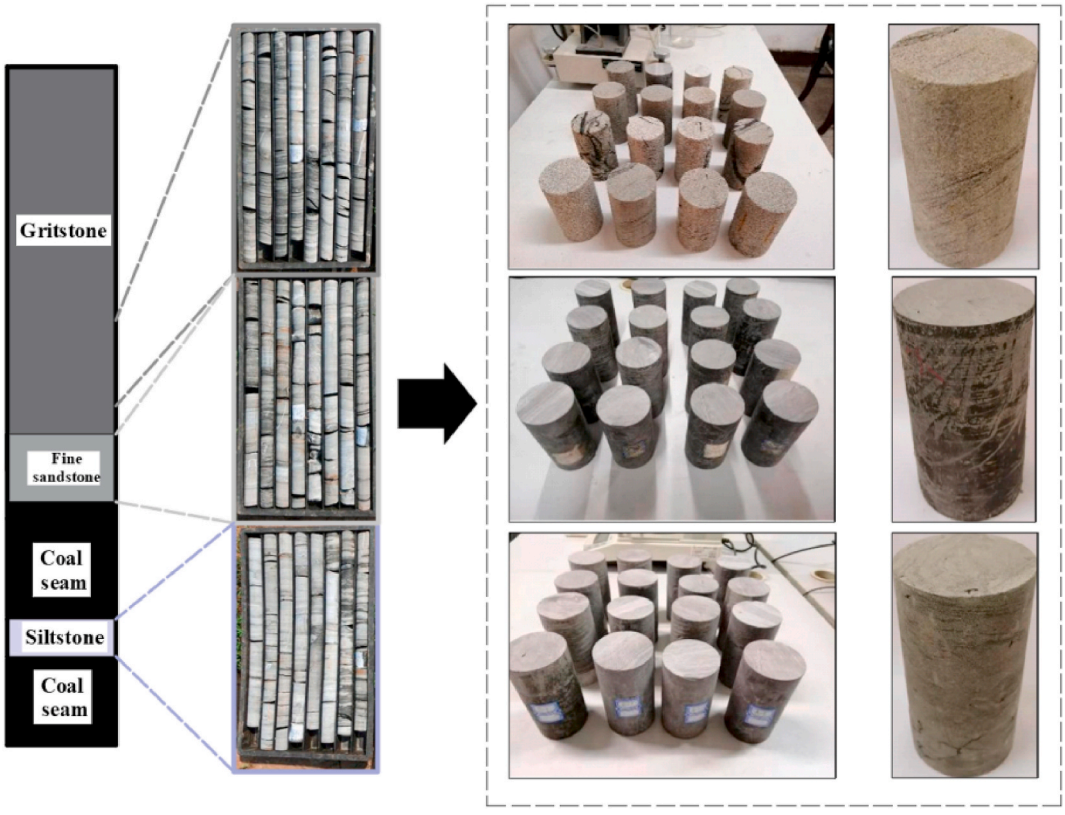

Fig. 2. The process of making samples of different types of sandstone.

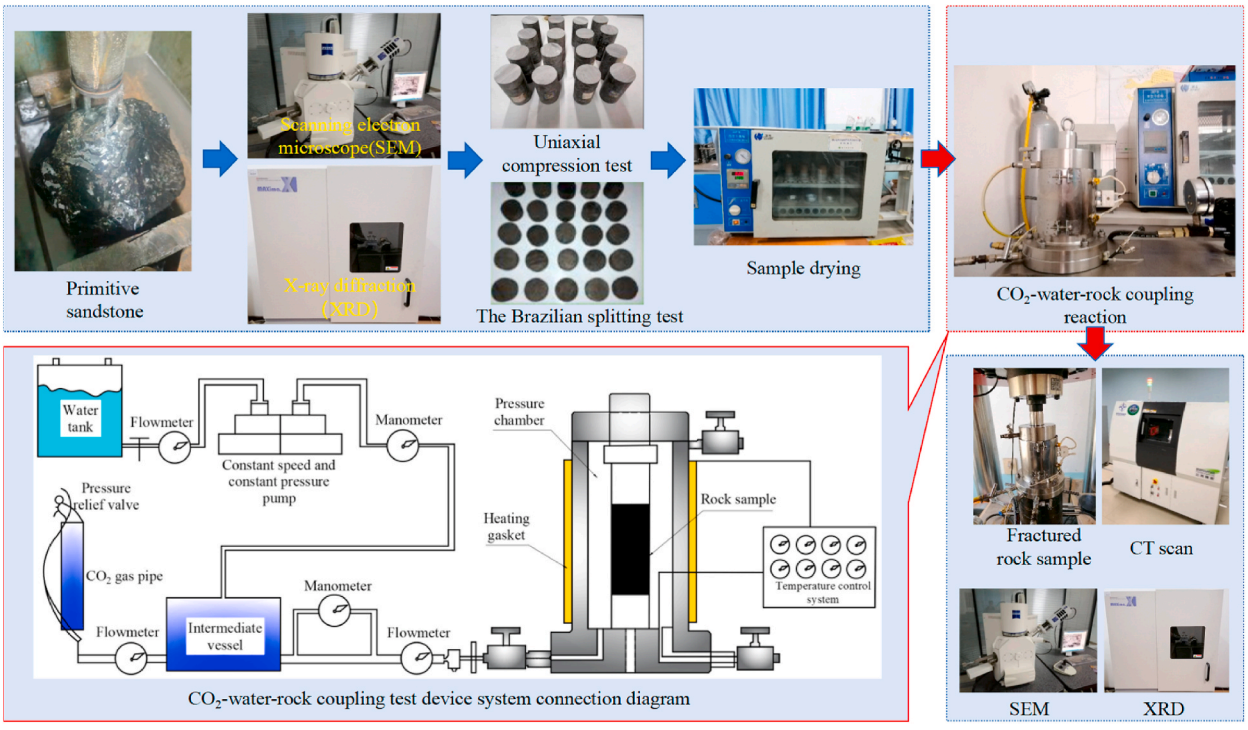

Fig. 3. CO_2-water-rock coupling test system [40].

the CO_2-coupled fracturing fluid configuration, a compounded surfactant consisting of anionic K-12 and nonionic OP-10 with a concentration of 2 ‰ was selected, and an aqueous KCl solution containing 2.5 % of KCl was added to the compounded surfactant, which was uniformly mixed and made into the active water-based solution, numbered CW-0, and the CO_2 cylinder was passed through to the CW-0 active water-based solution, using a constant temperature magnetic stirrer and adjusting the rotational speed, so that CO_2 is fully dissolved in the CW-0 active water-based solution until saturated, and the prepared CO_2 saturated solution continues to be added to the different quality of the CW-0 active water-based solution, and CO_2 coupled fracturing fluids with CO_2 mass fractions of 4 %, 6 %, and 8 % are configured respectively, with the numbering CW-4, CW-6, and CW-8, respectively. CW-4, CW-6 and CW-8, respectively.

2.2. CO_2-water-rock coupled fracturing system

The self-developed CO_2-water-rock coupling test device (Fig. 3) was used to test the mechanical properties and internal structural characteristics of rock samples before and after the coupling action. The device mainly consists of a pressure chamber, a temperature control system, a coupling fracturing fluid supply device, and a constant-speed and constant-pressure pump, etc. The maximum working pressure of the triaxial pressure chamber is 40.0 MPa, and a stress sensor is installed inside. The maximum working pressure of the triaxial pressure chamber is 40.0 MPa, and the stress sensor is installed inside. The heating device in the temperature control system wraps the side of the pressure chamber, and heats the pressure chamber through the heating ring and heat-insulating asbestos, and realizes the temperature control of the pressure chamber by using the built-in temperature sensors and controllers (room temperature to 100.0 °C), and the constant-speed and constant-pressure pump can realize the pressurization in the range of 0.0–40.0 MPa, and the constant-speed and constant-pressure pump can realize the pressurization in the range of 0.0–40.0 MPa. The pressure inside the pressure chamber is tracked in real time through the pressure gauge and stress sensor to ensure constant pressure.

2.3. CO_2-water-rock coupled fracturing experiments

The lithology and temperature-pressure environment of sandstone formations are important influencing factors for the evolution of their dynamic mechanical properties, however, the lithology of rocks is difficult to be changed by human intervention, therefore, physical damage and chemical erosion of rock bodies by changing the environment of rock formations have become one of the main means of artificially modifying the properties of rock formations [41]. In this experiment, the effects of CO_2 mass fraction, temperature, pressure, time and number of reaction cycles on the compressive and tensile strength of the rock mass during coupled fracturing experiments were mainly investigated, and the specific experimental conditions were as follows(Table 1).

In this study, the CO_2-water-rock coupling test was carried out, the temperature of the pressure chamber was set and the heating system was turned on, and after the temperature was stabilized to the set value, the inlet valve was opened, CO_2 was injected at regular intervals and quantitatively, the inlet valve was closed, the injection valve was opened, and the pressure was pressurized using the booster pump according to the pressurization rate of 0.3 MPa/min, and the pressure in the pressure chamber was maintained at a constant pressure until the pressure reaches the target value and the recording of the change rule of the tensile strength and compressive strength of the rock before and after the experiment started [43,44]. Tensile strength and compressive strength of the change rule, after the experiment, the samples were removed from the coupled reaction device, set in a drying oven at 60 °C to dry for 24h, and then sealed and preserved for other experiments. As shown in previous studies [45–47], siltstone has a denser pore structure, less pore volume and lower permeability than fine-grained sandstone and coarse-grained sandstone, and thus is theoretically the most difficult to be eroded by the infiltration of aqueous chemical solutions. Based on this, this paper firstly selects siltstone as the rock test sample to carry out the CO_2-water-rock coupling test, analyze the influence of key factors such as CO_2 volume fraction, reaction temperature, reaction time and pore pressure on the CO_2-water-rock coupling, and then carry out the test of fine-grained sandstone and coarse-grained sandstone samples based on the optimal test parameter conditions, to analyze the influence of lithology on the CO_2-water-rock coupling. The test will be conducted on fine-grained sandstone and coarse-grained sandstone samples to analyze the influence of lithology on CO_2-water-rock coupling.

2.4. Experiments on pore and fracture structure and component evolution in sandstone

Scanning electron microscope (SEM) was used to study the microstructure of the sandstone samples before and after the reaction (based on the results of the coupled fracturing experiments, the microscopic tests were only carried out on the samples with the best

Table 1
Experimental parameter conditions [40,42].

Factor	Experiment condition
Temperature	25 °C,35 °C,45 °C
Pressure	3 MPa,5 MPa,7 MPa
Time	6h,8h,10h
Cycle number	Once,3 times,7 times
CO_2 Mass fraction	4 %,6 %,8 %
Rock species	Siltstone; fine-grained sandstone; coarse-grained sandstone

softening effect after the test, hereinafter), in order to obtain the microscopic surface morphology of the natural rock samples. The scanning electron microscope test of the rock samples was carried out using a German Zeiss ZEISS Sigma 500 field emission scanning electron microscope with a high and low vacuum resolution of 0.8 nm and 1.4 nm, a magnification of 10 to 1 million times, and an accelerating voltage of 0.02–30 kV. After the start of the test, reduce the focusing power so that the sample can be clearly observed, move the sample stage, as far as possible to observe the sample surface pore fissure structure, adjust the brightness and contrast, so that the fluorescent screen display image brightness and darkness of the moderate image, image adjustment is clear, according to the magnification needed to take pictures.

A MAXima-XRD-7000 X-ray diffractometer (XRD) was used to determine the changes in mineral components of the samples before and after coupled fracturing. The testing process was carried out using Cu-target X-rays at an operating voltage of 40 kV and an operating current of 30 mA. Before scanning, the sample powder was placed horizontally on the carrier table, the scanning range of the vertical goniometer was adjusted to be 10–80°, and the scanning speed was set to be 3.85°/min. The X-ray diffractometer was turned on to conduct the test, and the X-diffracted bopper of the rock samples tested was analyzed using the JADE6.0 software. JADE6.0 software was used to analyze the X diffraction waveforms of the tested rock samples to obtain the mineral fraction profiles and elemental contents of each rock sample.

In this paper, the nanoVoxel-3000 geotechnical multi-scale high-resolution integrated scanning system was used to qualitatively and quantitatively analyze the pore and fissure structure and mineral evolution caused by CO_2-water-rock coupling, and the pore and fissure of the three sandstone specimens, namely, chalky sandstone (C-T-F), fine-grained sandstone (C-T-X), and coarse-grained sandstone (C-T-C), were segmented according to the dual-threshold segmentation method of the CT images, matrix and minerals segmented images for body rendering, and then build a 3D visualization model.

3. Results

3.1. Changing law of CO_2-water-rock coupling compressive strength

According to the stress-strain curves before and after the CO_2-water-rock coupling action (Fig. 4a), the change rule of the mechanical parameters of the rock samples can be obtained (Fig. 4b), compared with the natural samples, the compressive strength and modulus of elasticity of the rock samples under the action of immersed clear water samples and coupled fracking fluids with different CO_2 mass fractions showed different degrees of decreases, and the action of the clear water, CW-0, CW-4, CW-6 and CW-8 The decreases of compressive strength were 12.13 %, 16.21 %, 23.51 %, 31.33 % and 42.81 %, and the decreases of modulus of elasticity were 23.28 %, 29.31 %, 37.18 %, 42.56 % and 57.87 %, respectively.

The compressive strength and modulus of elasticity of the rock samples acted by CO_2-coupled fracturing fluid decreased more than that of the natural samples and water-soaked samples as a whole, and the larger the CO_2 mass fraction was, the more obvious the decrease of compressive strength and modulus of elasticity was, so it can be seen that the CO_2-water-rock interaction contributed to the mechanical damage of the rock body, and the coupled fracturing fluid with a CO_2 mass fraction of 8 % (CW-8) had the most significant effect on the weakening of the strength of the rock samples.

3.2. Changing law of CO_2-water-rock coupling tensile strength

Since the tensile strength and compressive strength have the same rule of change, it can be seen that among the various fracturing fluids, CW-8 can make the tensile strength of the rock to produce the largest degree of decline. Therefore, this paper focuses on the influence in temperature field, stress field and action time on the tensile strength of sandstone under the action of CW-8. The characteristic curves of sample loading with reaction time under different reaction temperatures, pore pressures, total time of static action and number of cycles were plotted respectively (Fig. 5).

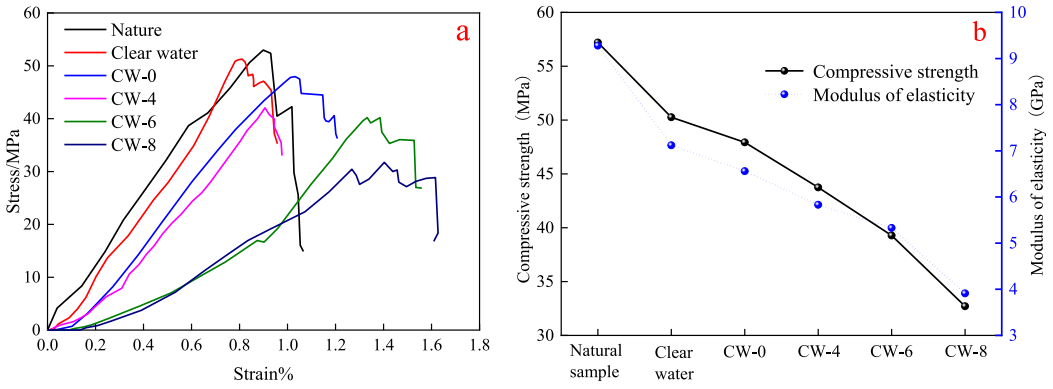

Fig. 4. Mechanical parameters of rock samples under different action conditions (a represents the stress-strain curve of the sample, and b represents the trend of mechanical property changes).

Regardless of the temperature, the tensile strength of the reacted sandstone samples showed a significant decrease compared with that of the natural rock samples (Fig. 5a), of which, the tensile strength decreased by 2.63 MPa, 57.21 %, the largest decrease at 25 °C, 1.66 MPa, 36.17 %, and 1.32 MPa, 28.76 %, the smallest decrease at 45 °C. The effect of CO_2-water-rock coupling showed a weakening trend with the increase of reaction temperature. 1.32 MPa, with a decrease of 28.76 %, the smallest decrease. The effect of CO_2-water-rock coupling shows a weakening trend with the increase of reaction temperature.

Pore pressure has a greater influence on the effect of CO_2-water-rock coupling, and the tensile strength of rock samples after coupling decreases with the increase of pore pressure (Fig. 5b). Compared with the natural rock samples, the tensile strength decreased by 20.47 % at a pore pressure of 3.0 MPa, 49.67 % at a pore pressure of 5.0 MPa, and 57.21 % at a pore pressure of 7.0 MPa, and the time for each sample to reach the peak load became shorter.

Overall, the decrease in tensile strength of the samples gradually increased with the growth of CO_2-water-rock coupling (Fig. 5c). When the action time increases from 0 to 6.0 h, the tensile strength decreases by 1.84 MPa, with a decrease rate of 5.0×10^{-3} MPa/min, compared to the natural rock samples with a decrease rate of 40.9 %, when the action time increases from 6.0 to 8.0 h, the tensile strength decreases by 0.12 MPa, with a decrease rate of 1.0 × 10-3 MPa/min, compared to the natural rock samples with a decrease rate of 42.71 %, when the action time increased from 8.0h to 10.0h, the tensile strength decreased by 0.67 MPa, the decrease rate was 5.6 × 10-3 MPa/min, compared with the natural rock samples, the decrease rate was 57.21 %, compared with the natural rock samples, the CO_2-water-rock coupling effect made the tensile strength of the rock samples to be decreased greatly, the process of coupling, with the increase of the action time, the rock samples gradually decreased the tensile strength. During the coupling process, the tensile strength of rock samples decreased gradually with the increase of the action time. Similar to the weakening effect in temperature and pore pressure on the strength of rock samples, the time for rock samples to reach the peak load value became shorter under each action time, and the longer the action time, the shorter the time for rock samples to reach the peak load value. Compared with temperature and pore pressure, the weakening effect of CO_2-water-rock coupling time on the tensile strength of rock samples is more significant.

Compared with the original samples, the peak load value of sandstone after CO_2-water-rock coupling decreased significantly, and the time to reach the peak value became shorter (Fig. 5d), and the more the number of cycles, the smaller the peak load value of the rock samples could be reached, and the shorter the time used, but compared with the difference in the peak stress value and the time used to reach the peak stress value before and after the action, the change of the tensile strength of the sandstone under the condition of different number of cycles was relatively small. The change in tensile strength of sandstone under different number of cycles is

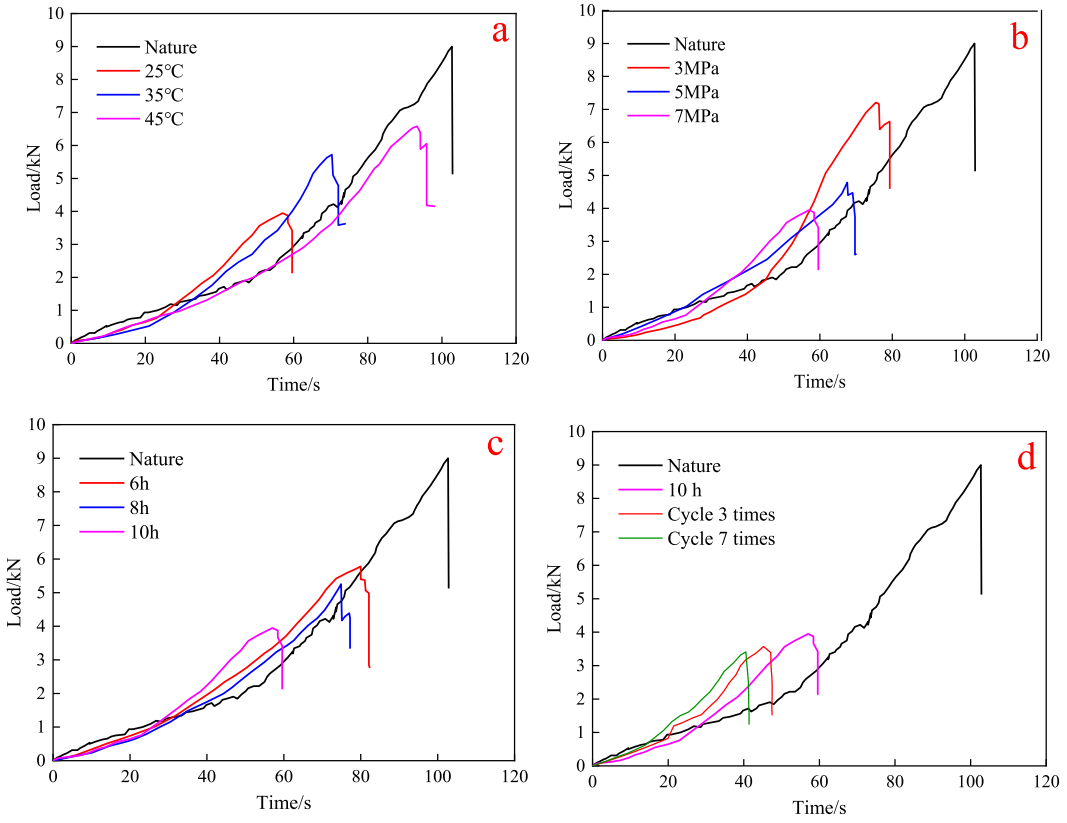

Fig. 5. Load evolution pattern of rock samples under different action conditions (a,b,c and d represent the characteristic curves of sample load variation with reaction time under the conditions of reaction temperature, pore pressure, total time of static action and number of cycles, respectively).

relatively small compared to the difference between the peak stress and the time taken to reach the peak stress.

The synthesis of the above experimental data and analysis shows that the tensile strength of the siltstone samples can be minimized by choosing the CW-8 coupling solution and softening the siltstone samples for 10.0h (cycling 1 time) under the conditions of the reaction temperature of 25 °C and the pore pressure of 7 MPa.

3.3. Effect of CO_2-water-rock coupling on the tensile strength of three sandstones

Based on the optimal experimental conditions for siltstone, Brazilian splitting tests after CO_2-water-rock coupling were carried out on two rock samples, fine-grained sandstone and coarse-grained sandstone, with the reacted siltstone, fine-grained sandstone, and coarse-grained sandstone specimens numbered B-1, X1-1, and C1-1, respectively. The splitting damage strength characteristics and morphology of the three sandstone specimens were compared with those of natural specimens F1, X1, and C1 (Fig. 6a).

After the coupling effect, the tensile strength of X1-1 and C1-1 samples decreased dramatically by 53.73 % and 46.65 %, respectively, compared with the natural samples. According to the Brazilian cleavage cumulative energy formula [48], the peak energy rate of the three samples was calculated and compared with the peak energy rate of the natural samples (Fig. 6b), compared with the natural rock samples, the peak energy rate of the siltstone sample B-1 decreased by 253 J/m^2 by 37.8 %, fine-grained sandstone by 277 J/m^2 by 48.2 %, and coarse-grained sandstone by 278 J/m^2 by 49.9 %.

3.4. Surface morphology evolution

The experiments used siltstone, fine-grained sandstone and coarse-grained sandstone samples (No. FSY-1, XLY-1 and CLY-1), which were put into the pressure chamber for CO_2-water-rock coupling respectively, and the coupling conditions were as follows: CW-8 coupling fracturing fluid, temperature of 25 °C, pore pressure of 7 MPa, and time of operation of 10.0h. Fig. 7a shows the surface morphology of the siltstone sample before the coupling reaction, which is magnified 2000 times by the scanning electron microscope. Fig. 8a shows the surface morphology of the fine-grained sandstone before the coupling reaction. Fig. 9a shows the surface morphology of the coarse-grained sandstone before the coupling reaction. Figs. 7b– 8b and 9b show the surface morphology of siltstone, fine-grained sandstone and coarse-grained sandstone after coupling reaction, respectively.

Comparing the surface microstructure of the rock samples before and after the coupling effect, it can be clearly seen that before the coupling effect, there are fewer cracks on the surface, mostly single cracks, with smaller pore diameters, lower degree of pore development, poorer connectivity between the pores, flatter surface, and minerals filling in the pores and cracks, as shown in Figs. 7a–8a and 9a. After the coupling effect, the rock samples are divided into different sizes of block or scale-like structure by the pores and fissures, the minerals in the pores are dissolved and eroded, the number of pores increases, the pore diameter becomes larger, the degree of development obviously improves, locally visible dissolved holes and cavities appear, most of the pores form inter-connected network channels, the effective volume of the original fissures becomes larger, accompanied by the generation of new fissures with different widths and lengths, irregularly distributed, and The effective volume of the original fractures becomes larger, accompanied by the generation of new fractures with different widths and lengths and irregular distribution, and evolves into a fracture network(Figs. 7b–8b and 9b), which improves the connectivity of the fracturing fluid seepage and diffusion channels.

3.5. CO_2-water-rock coupling mineral composition change

X-diffraction tests were conducted for the mineral fractions of the three rock samples after CO_2-water-rock coupling, and component data (Table 2) and plots (Fig. 10) were obtained for the sandstones.

The original samples of the three sandstones contain more quartz and clay minerals, and the rest of the mineral components contain

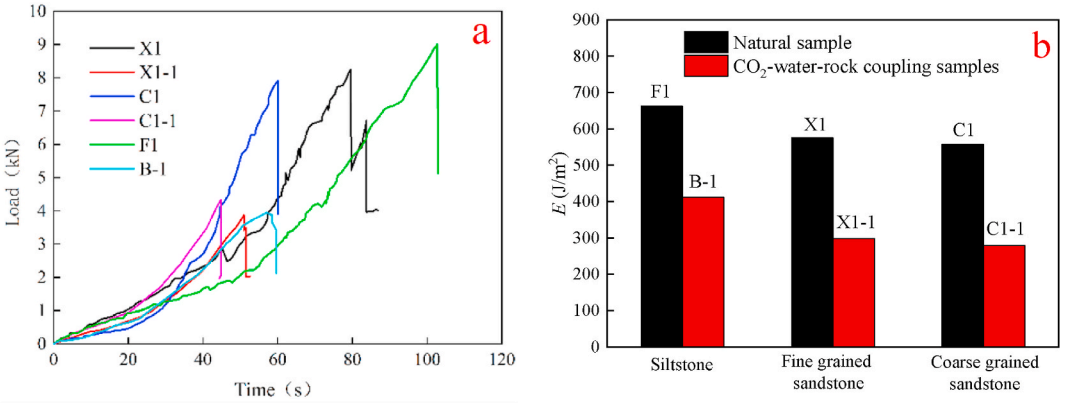

Fig. 6. Comparison of load and energy rate before and after the coupling effect of different samples (a and b represent the change patterns of load and energy rate of samples, respectively).

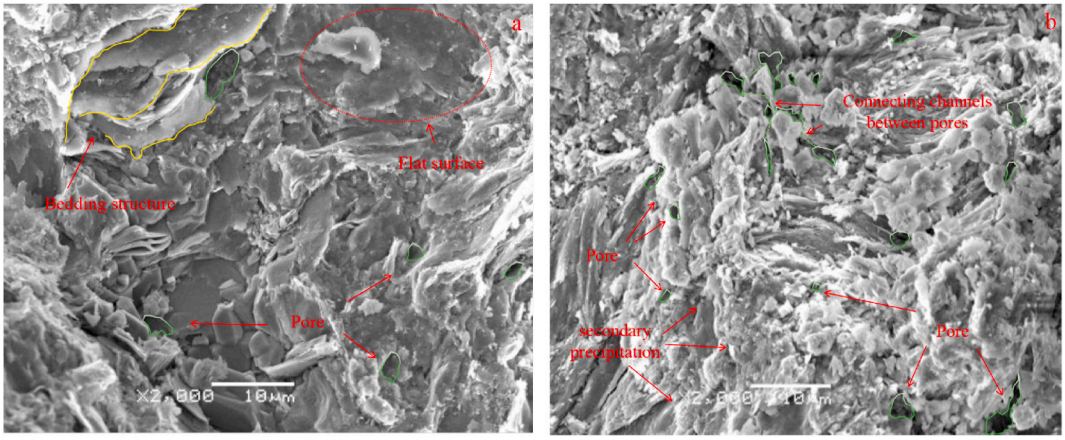

Fig. 7. Changes in surface morphology of siltstone before and after coupling (a and b represent the coupling before and after action, respectively).

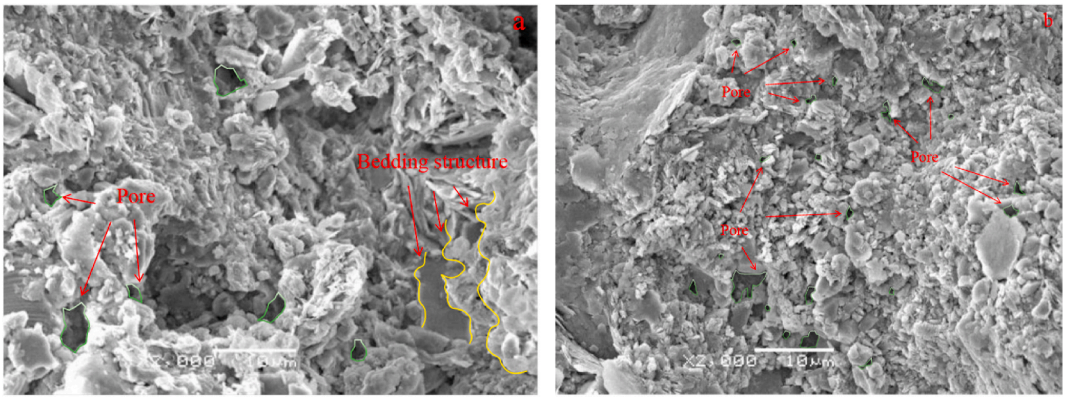

Fig. 8. Changes in surface morphology of fine-grained sandstone before and after coupling (a and b represent the coupling before and after action, respectively).

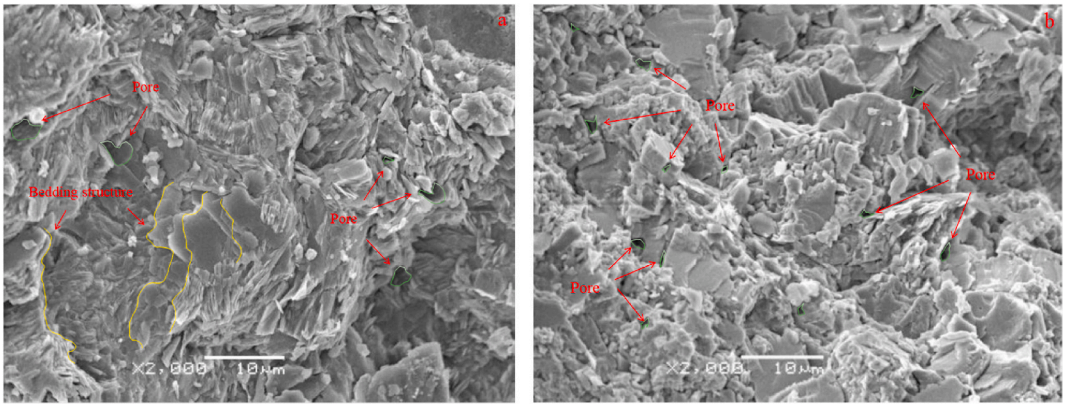

Fig. 9. Changes in surface morphology of coarse-grained sandstone before and after coupling (a and b represent the coupling before and after action, respectively).

less. After the CO_2-water-rock coupling, on the whole, the calcite, dolomite, and sodium feldspar in the three rocks show a decreasing tendency, and the contents of quartz and clay minerals have been further elevated. After the siltstone specimen was acted by the CW-4 coupled fracturing fluid, the dolomite content decreased from 6.21 % to 5.35 %, which was a small decrease; calcite increased from 7.31 % to 7.96, which indicated that there was the generation of calcite in the dissolution reaction, and the precipitation effect was

Table 2
Test results of mineral fraction before and after CO_2-water-rock coupling.

Sample Name	Sample state	Quartz(wt %)	Calcite(wt %)	Dolomite(wt %)	Sodium feldspar (wt%)	Pyrite(wt %)	Clay minerals(wt %)
Siltstone sample	Original shape	59.37	7.31	6.21	5.27	8.89	12.95
	CW-4	60.15	7.96	5.35	4.62	7.16	14.76
	CW-6	63.73	5.27	4.61	4.12	6.35	15.92
	CW-8	67.45	1.19	1.06	2.75	3.93	23.62
Fine-grained sandstone sample	Original shape	67.93	6.91	5.75	2.23	3.81	13.37
	CW-8	69.91	0.75	1.33	0.91	2.37	24.73
Coarse sandstone sample	Original shape	71.03	3.22	5.75	7.31	3.78	8.91
	CW-8	71.95	0.19	0.96	3.52	1.86	21.52

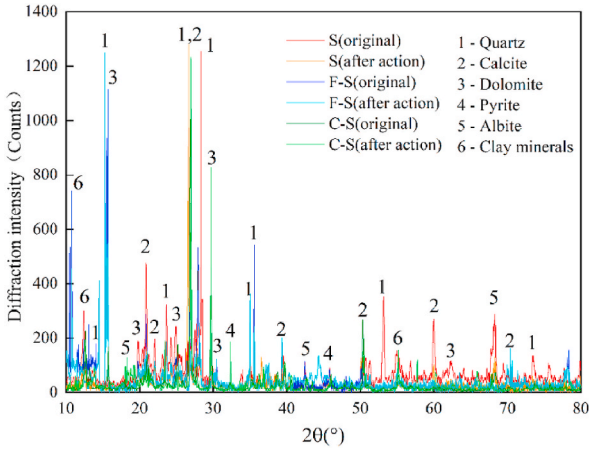

Fig. 10. XRD analysis of CO_2-water-rock coupling in three sandstone samples.

greater than the dissolution effect; the contents of sodium feldspar and pyrite both had a small decrease, which decreased by 0.65 % and 1.73 %, respectively; along with the dissolution of dolomite, sodium feldspar and pyrite, quartz and clay minerals increased to some extent, by 0.78 % and 1.81 %, respectively. When the coupling fracturing solution is CW-6, compared with CW-4, the acidity of the solution becomes stronger, and it can be found that the calcite content decreases from 7.31 % to 5.27 % after the action, which indicates that the coupling solution has dissolved calcite; dolomite, sodium feldspar and pyrite continue to show a weaker decreasing trend, compared with the CW-4 coupling fracturing solution, which decreases by 0.74 %, 0.5 % and 0.81 %, respectively; quartz and clay minerals continued to rise. When the coupling fracturing fluid is CW-8, the acidity of the solution is further enhanced, and the peak intensities of calcite and dolomite are significantly lower than those in other conditions on the X-diffraction pattern; the contents of sodium feldspar and pyrite are decreased by 2.52 % and 4.96 %, respectively, compared with that of natural samples; compared with the other conditions, the contents of quartz and clay minerals reach a high level, increasing to 67.45 % and 23.62 %, respectively, and the contents of clay minerals increase to 67.45 % and 23.62 %, respectively, and the contents of quartz and clay minerals continue to rise. and 23.62 %, with the most obvious increase in clay mineral content. It can be seen that with the increase of CO_2 mass fraction, the degree of dissolution and solubilization of siltstone minerals intensified, among which, the solubilization of calcite was the highest, dolomite was the second, and sodium feldspar and pyrite were the lowest in CW-8, and the solubilization of minerals was greater than the precipitation.

Coarse-grained sandstone samples after coupling action almost undetectable calcite and dolomite peaks, indicating that the two minerals have been dissolved, as can be seen from Table 2, the calcite content decreased from 3.22 % to 0.19 %, and dolomite content decreased from 5.75 % to 0.96 %; sodium feldspar content decreased to 3.52 %, which is 51.8 % lower compared with the natural samples; pyrite has also undergone a more pronounced dissolution The pyrite also had a more obvious dissolution reaction, the content decreased from 3.78 % to 1.86 %; the quartz content increased by 0.92 %, and the clay mineral content increased most obviously, compared with the natural samples increased by 12.61 %.

In summary, it can be seen that CO_2-water-rock coupling can make the mineral components of the constituent rocks undergo complex reactions such as dissolution and precipitation. Under certain conditions, the erosion is greater than the precipitation, especially for carbonate minerals, which makes the pore size larger, produces secondary pores, and further improves the complexity of microscopic pores, which effectively unblocks the pore and crack channels and improves the permeability of sandstone. The CO_2-water-rock coupling chemical damage mechanism will be further discussed in Section IV.

3.6. Splitting morphology and three-dimensional reconstruction of sandstone samples after coupling effects

In this study, the splitting failure modes of three rock samples before and after CO_2-water-rock coupling are compared and sorted out. Fig. 11a shows the failure mode of the original sample of siltstone after splitting. Fig. 11b shows the failure mode of the original sample of fine-grained sandstone after splitting. Fig. 11c shows the failure mode of the original sample of coarse-grained sandstone after splitting. Fig. 11d–. e and f show the splitting failure modes of siltstone, fine-grained sandstone and coarse-grained sandstone samples after CO_2-water-rock coupling.

Before the coupling effect, the destruction of siltstone (Fig. 11a), fine-grained sandstone (Fig. 11b) and coarse-grained sandstone (Fig. 11c) specimens all formed an obvious main cleavage, which cracked along the sides of the loading diameter, with the main cleavage smooth, and the presence of secondary cleavage was not obvious, and the three sandstone specimens belonged to typical brittle damage. After the coupling action of the samples in the B-1 (Fig. 11d) specimen in the direction parallel to the radial loading diameter appeared in a number of primary cracks, the main crack is jagged and accompanied by a number of secondary cracks, X1-1 (Fig. 11e) rock samples along the direction of the diameter of the loading to form a main crack, the center of the end face of the tensile damage, compared with the X1 specimen, X1-1 specimen formed a larger width of the main cracks, and the end face of the specimen is first compression damage to the formation of secondary cracks, the C1-1 (Fig. 11f) specimen of the two main cracks are intersected and extended in a corrugated shape, and the damage range is roughly spread along the contact surface of arc loading, and the secondary cracks are not obvious. The complexity of the deformation and damage characteristics of the rock samples is directly related to the CO_2-water-rock coupling.

Figs. 12–14 give the three-dimensional reconstruction results of the splitting morphology of each rock sample before and after CO_2-water-rock coupling. According to the structural characteristics of the distribution of pores and fissures in different rock samples, different colors are used to represent the pores and fissures and mineral areas in the rock samples. Fig. 12a and b show the three-dimensional reconstruction results of siltstone before and after CO_2-water-rock coupling. Figs. 12c and d show the three-dimensional reconstruction results of fine-grained sandstone before and after CO_2-water-rock coupling. Figs. 12e and f show the three-dimensional reconstruction results of coarse-grained sandstone before and after CO_2-water-rock coupling. Consistent with the display order of Figs. 12 and 13 (a-f) shows the pore fracture distribution of the three sandstone samples before and after the reaction, and Fig. 14 (a-f) shows the internal mineral composition of the three sandstone samples before and after the reaction.

It is found that the three-dimensional structure of sandstone has changed slightly before and after the reaction (Fig. 12), and there are a lot of pores, fissures (Fig. 13) and mineral precipitation (Fig. 14) in the rock. , in order to quantitatively study the effect of CO_2-water-rock coupling on the three-dimensional structure of the pores and cracks inside the rock, in this paper, we equated each independent pores and cracks inside the rock samples as a sphere equal to its volume, and the equivalent radius of the independent pore-slit is calculated as [49]:

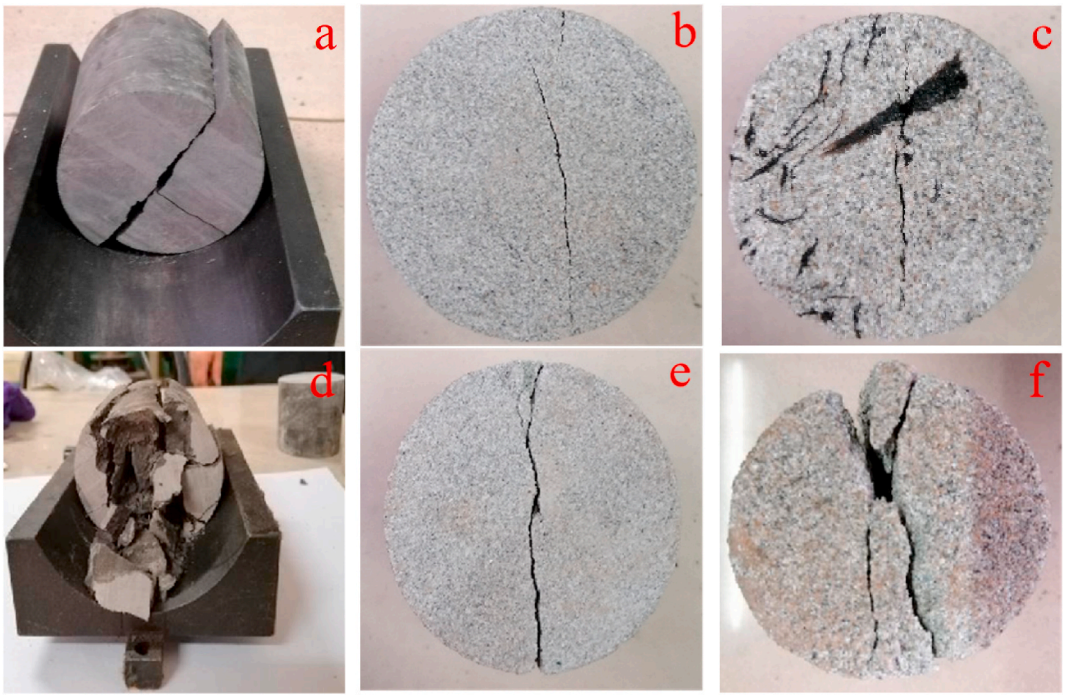

Fig. 11. Comparison of Brazilian splitting damage patterns of sandstone samples before and after CO_2 - water-rock coupling (a,b,c represent the splitting patterns of the three samples before the coupling effect, and d,e,f represent the splitting patterns of the samples after the coupling effect, respectively).

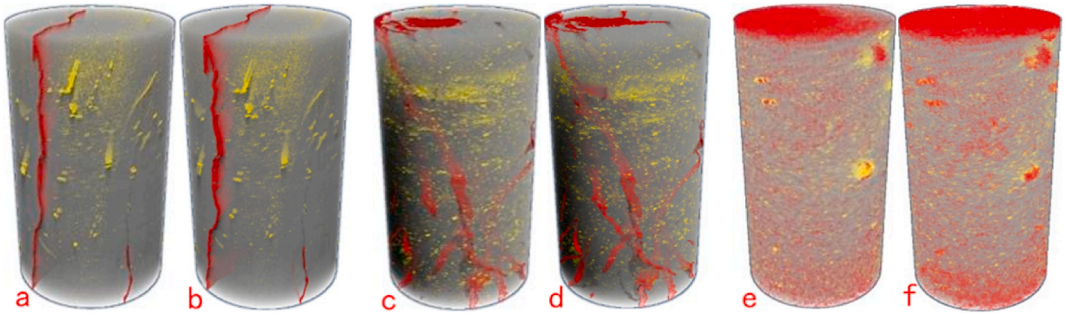

Fig. 12. Results of 3D reconstruction of samples before and after reaction (a and b represent 3D reconstruction of siltstone samples before and after reaction, respectively; c and d represent 3D reconstruction of fine-grained sandstone samples before and after reaction; and e and f represent 3D reconstruction of coarse-grained sandstone samples before and after reaction).

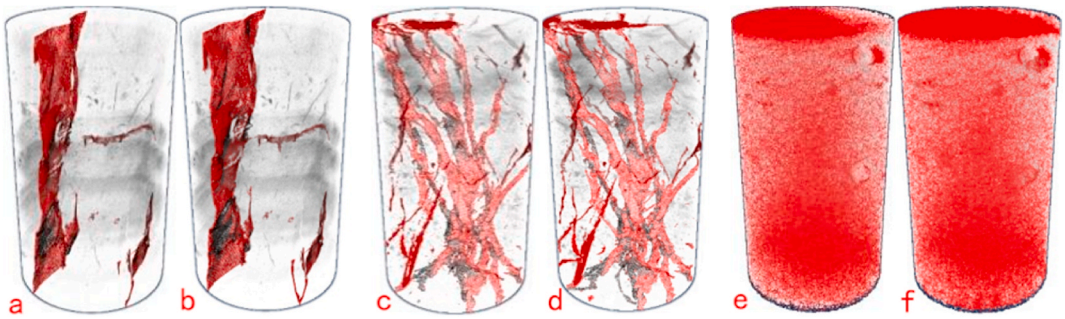

Fig. 13. Pore cleavage before and after sample reaction (a and b indicate pore cleavage before and after reaction of siltstone samples, respectively; c and d indicate pore cleavage before and after reaction of fine-grained sandstone samples; e and f indicate pore cleavage before and after reaction of coarse-grained sandstone samples).

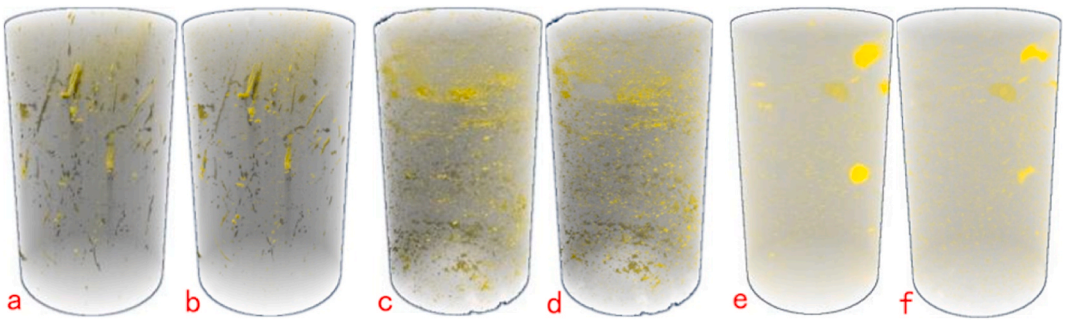

Fig. 14. Minerals before and after sample reaction (a and b represent internal minerals before and after the reaction of the siltstone sample, respectively; c and d represent internal minerals before and after the reaction of the fine-grained sandstone; and e and f represent internal minerals of the coarse-grained sandstone).

$$r = \frac{d_{eq}}{2} = \frac{\sqrt[3]{6V_P/\pi}}{2} \tag{1}$$

where d_{eq} is equivalent diameter of the pore-crack structure, V_P is Volume of the independent pore-crack structure.

Subsequently, the volume fractions of pore-slit and mineral are extracted, and the volume fractions of pore-slit and mineral are the ratios of the total volume of the pore-slit space pixels and the total volume of the mineral space pixels to the volume of the rock samples, respectively, and the pore-slit volume fractions can characterize the degree of overall damage destruction of the rock samples by the coupling effect, and the mineral volume fractions can characterize the degree of chemical damage of the rock samples by the coupling effect.

Based on the principle of fractal geometry, the density function of the pore-crack radius distribution of porous media is [50]:

$$f(r) = cr^{-D_V-1} \tag{2}$$

where c is constant of proportionality, D_V is pore-slit volume fractal dimension.

Based on the assumption of the equivalent sphere model, the cumulative pore-fracture volume within the rock sample with a pore-fracture radius less than r can be obtained V_r:

$$V_r = \int_{r_{\min}}^{r} f(r)ar^3 \mathrm{d}r = \frac{ac}{3-D_V}\left(r^{3-D_V} - r_{\min}^{3-D_V}\right) \tag{3}$$

where $r_{\min}$ is minimum pore-slit radius in a rock sample; a is constant of proportionality.

And the total pore-crack volume of the specimen is:

$$V = \frac{ac}{3-D_V}\left(r_{\max}^{3-D_V} - r_{\min}^{3-D_V}\right) \tag{4}$$

It is known that the percentage S_V of pore fracture volume with pore fracture radius less than r to the total cumulative pore fracture volume is:

$$S_V = \frac{r^{3-D_V} - r_{\min}^{3-D_V}}{r_{\max}^{3-D_V} - r_{\min}^{3-D_V}} \tag{5}$$

Since the internal pore-crack structure of sandstone has strong inhomogeneity, the pore-crack radius tends to have a large difference, so the size of $r_{\min}$ is negligible, which can be obtained as

$$S_V = \left(\frac{r}{r_{\max}}\right)^{3-D_V} \tag{6}$$

Taking the logarithm of equation (5) yields:

$$\ln(S_V) = (3-D_V)\ln(r) + c' \tag{7}$$

where $c'=(D_V\text{-}3)\ln(r_{\max})$, then the pore-crack volume fractal dimension $D_V = 3\text{-}k$, the size is between 2 and 3.

The volume fractions of pore fissures and minerals inside the rock samples before and after CO_2-water-rock coupling were extracted and their fractal dimensions were obtained (Table 3), and it can be seen that the inside of each sandstone specimen contains pre-existing pore fissures and mineral impurities, and compared to the pore fissures, the volume fractions and fractal dimensions of mineral impurities in each rock sample before CO_2-water-rock coupling are larger, and the inside of the samples have higher mineral contents and more structural morphology. The volume fraction and fractal dimension of the mineral impurities are larger, the mineral content inside the rock samples is higher, and the structural morphology is more complicated. After the coupling, the volume fraction of pore space of siltstone, fine-grained sandstone and coarse-grained sandstone increased by 1.71 %, 1.96 % and 0.79 %, respectively, and the volume fraction of minerals decreased by 0.44 %, 0.58 % and 0.28 %, respectively, and the fractal dimensions of the three kinds of sandstone samples' pore space increased to different degrees, while the volume fraction of minerals and fractal dimensions decreased.

The data in Table 3 visualize the results of the evolution of the internal pore-crack structure and minerals in each rock sample after CO_2-water-rock coupling, which is corroborated by the quantitative information of the internal structure of CO_2-water-rock coupling listed in Table 3. The change of the internal pore-crack body of the rock caused by the coupling action also dramatically increased the complexity of the pore-crack distribution, and, at the same time, further verified the dissolution and melting of the mineral skeleton and particles in the sandstones by the CO_2-water-rock coupling action.

4. Discussion

4.1. Dynamic mechanical influences on sandstone under coupled action

The mechanical deterioration of sandstone in CO_2-water-rock coupling is manifested in the change of tensile strength of samples.

Table 3
Quantification of the internal structure of each rock sample based on coupling interaction.

Sample numbering	Coupling action	Pore fracture characteristics		Mineral characteristics	
		Volume fraction(%)	The fractal dimension	Volume fraction(%)	The fractal dimension
C-T-F	Original shape	1.05	2.11	2.07	2.32
	CW-8	2.76	2.45	1.63	2.25
C-T-X	Original shape	1.13	2.19	2.35	2.49
	CW-8	3.09	2.51	1.77	2.16
C-T-C	Original shape	0.92	2.07	1.61	2.20
	CW-8	1.71	2.26	1.33	2.12

Therefore, in this study, the evolution patterns of sandstone tensile strength with different coupling conditions were fitted separately, and the relationships between the evolution patterns of sandstone tensile strength and different reaction temperatures, pore pressures, action times and number of cycles were obtained (Fig. 15).

Temperature has a certain effect on the tensile strength of rock samples after CO_2-water-rock coupling (Fig. 15a), as shown in Fig. 15a), with the increase in temperature, the viscosity of CO_2 coupled fracturing fluid decreases and the permeability coefficient increases, according to Darcy's law, under a certain pore pressure and permeable area of the pressure chamber, the permeability flow rate increases, and the coupled fracturing fluid has an enhanced wetting effect on the rock samples, which reduces the strength of the rock body. However, according to the experimental results, the tensile strength increases when the temperature increases, which is due to the fact that the increase in temperature makes the CO_2 solubility in water decrease, the pH of the CO_2 coupled fracturing fluid increases, the acidity decreases, and the chemical damage effect of the coupled fracturing fluid on the rock body is reduced to a certain extent. The temperature effect on the tensile strength of the sandstone is a joint result of the physical wetting effect of the fracturing fluid and the acid corrosion effect.

Fig.15 b shows the variation of compressive strength of sandstone samples with pore pressure. The results show that the increase of pore pressure affects the physical and chemical properties of CO_2-coupled fracturing fluid. Under the action of pore pressure, the sandstone is compressed and produces initial compression damage, which reduces the effective stress in the rock body, and under the strong adsorption of CO_2, the sandstone specimen produces a certain degree of expansion and deformation, which leads to expansion and deformation damage, and after the completion of the pressurized immersion, although the peripheral pressure has been unloaded, the pore pressure inside the specimen can not be unloaded within a short period of time, and the adsorption in the internal pore pressure can not be unloaded. And adsorbed in the internal pore fissures in the CO_2 can not completely escape, will still produce damage to the rock samples, the greater the pore pressure, the stronger the role of this damage, in addition, in the case of the temperature remains unchanged, with the increase in pore pressure, the CO_2-water system pH value decreases, acidity is enhanced, the chemical effect of some minerals from the sandstone internal extraction and organic matter, so that the composition of the minerals and the rock particles size, shape Changes occurred, the change on the one hand, the sandstone native pore and fracture structure expansion, on the other hand, in the microstructure of the rock samples to promote a part of the pore and fracture emergence and development (Figs. 9 and 13), and ultimately weakened the macro-mechanical properties of sandstone specimens.

It can be found through Fig. 15c that the longer the CO_2-water-rock coupling action, the greater the decrease in sandstone compressive strength, through a longer period of coupling action, on the one hand, it can sufficiently improve the macroscopic physico-

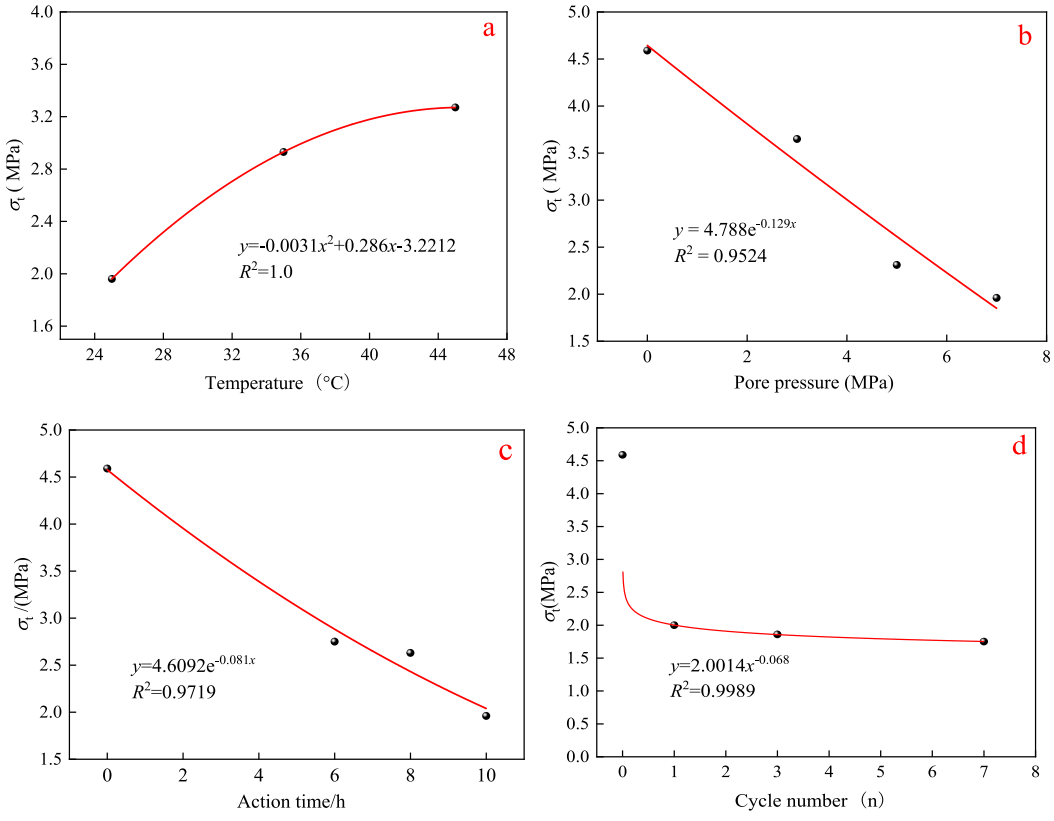

Fig. 15. Trend fitting of tensile strength of samples with different reaction conditions (a, b, c and d represent the variation of peak stress of tensile strength of samples with different reaction temperatures, pore pressures, action time and number of cycles, respectively).

mechanical properties of the rock body to ensure that the mechanical strength of the rock samples get the maximum degree of deterioration, on the other hand, the sandstone in the injection of high-pressure CO_2 coupled fracturing fluid, the cleavage action of the cracks produced cracks or make the natural cracks On the other hand, under the injection of high-pressure CO_2 coupling fracturing fluid, the splitting action of sandstone produces cracks or restarts the natural cracks, which further promotes the improvement of the overall structure and permeability of the rock formation, and the formation of a complex crack network, thus improving the crushing and softening effect. However, we can see from Fig. 15d that the coupling action caused damage to the internal cracks of sandstone, and after the initial action, the cracks developed and expanded, and the permissible deformation of the rock body increased, and the deformation amount reached a higher value at one time, and with the increase in the number of cycles, the deformation amount generated by the temperature stress and the chemical coupling action gradually stabilized, and the development of the internal pore cracks of the rock body was suppressed, so that the influence of the number of cycles on the tensile strength of the rock body was gradually reduced. decreases.

4.2. CO_2-water-rock coupled chemical-mechanical damage mechanism

The pore structure characteristics and mineral fraction composition of the rock body are the microscopic direct reflection of CO_2-water-rock coupling [33], therefore, this work aims to study and discuss the pore structure properties and mineral fraction characteristics of the samples before and after the coupling interaction. Since the sandstone selected in this paper contains a large number of primary pores and fractures, which provides space for the coupled CO_2-water-rock reaction, when the coupled fracturing fluid is injected into the rock body, it will flow along these pore-fracture systems. The chemical reaction between the fracturing fluid and the carbonate minerals generates soluble salts, which are carried away with the continued flow of the fracturing fluid, resulting in the dissolution of the minerals that originally supported the pore-fracture structure [51], and the structural changes caused by this chemical action include not only the increase in pore volume and the number of pores, but also the fracture expansion. These changes ultimately make the pore-fracture structure of sandstone reservoirs more complex and irregular, reducing the effective stress-transfer paths, thereby decreasing the strength and shear strength of the rock and making sandstone more susceptible to mechanical damage from subsequent production activities [52]. The mineral fractions in the sandstones studied in this paper that are capable of mineralization with CO_2-coupled fracturing fluids include mainly feldspar, calcite and clay minerals (Table 4).

(1) Reaction of feldspar and calcite with CO_2-coupled fracturing fluid

For $KAlSi_3O_8$ and $NaAlSi_3O_8$ in potassium feldspar and plagioclase feldspar, $CaAl_2Si_2O_8$ reacts with H^+ in CO_2-coupled fracturing fluids (equations 8-10), feldspar reacts with H^+ to generate kaolinite and quartz as two kinds of secondary minerals, and releases metal cations, in which the Ca^{2+} reacting with $CaAl_2Si_2O_8$ in plagioclase feldspar can generate calcite precipitates with CO_3^{2-}, and if the mass fraction of CO_2 in the coupled fracturing fluid is increased appropriately, the calcite precipitates will be formed. Ca2+ can generate calcite precipitation with CO_3^{2-}, if the mass fraction of CO_2 in the coupled fracturing fluid is increased appropriately, calcite can continue to react to generate $Ca(HCO_3)_2$; in addition, kaolinite and Na^+ react to generate sodium alumina precipitation (equation 11), and dolomite ($CaMg(CO_3)_2$) and calcite belong to the carbonate minerals, but compared to calcite, it is more slow in reacting with H^+, and it has a higher reaction rate with H^+, and it is also a carbonate mineral, and the reaction rate with H+ is slower. The reaction rate is slower than that of calcite, and metal cations are formed upon reaction with H^+ (Formula 12), where Ca^{2+} reacts with $HCO3^-$ to form calcite precipitates and Mg^{2+} reacts with $HCO3^-$ to form magnesite precipitates.

Calcite (CaCO3) is highly susceptible to react with H^+ in CO_2 coupled fracturing fluids to release Ca^{2+}, which in turn generates secondary calcite in the presence of a large CO_2 mass fraction (equation 12).

(2) Reaction of clay minerals with CO_2-coupled fracturing fluid

The content of clay minerals in the sandstones studied in this paper accounts for a relatively large amount of clay minerals, and the XRD test results (Table 2) show that the clay minerals of the three sandstone specimens include kaolinite, illite, and chlorite, kaolinite has a high stability in acidic solutions, illite and chlorite will precipitate metal cations when they react with H+ (Formula 13), and kaolinite is also generated from the reaction between illite and chlorite and H+, therefore, the kaolinite is both a primary and secondary mineral. Under the action of coupled fracturing fluid, clay minerals not only precipitate crystals (e.g., kaolinite precipitation) after reaction, but also swell in water, increase in volume, block pore fissures and roar channels, and reduce porosity and permeability.

In summary, the chemical effect of CO_2 coupled fracturing fluid on the rock body is mainly due to the dissolution of CO_2 in water to form carbonic acid, and the first-order ionization constant of carbonic acid in the CO_2-water system causes the acidity of coupled fracturing fluid to be enhanced, and the coupled fracturing fluid and the carbonate minerals in the rock undergo dissolution, solubilization, and precipitation, which opens up pore fractures that are in a closed or semi-closed state, resulting in the widening of the original pore space and the through passage of the pore fracture. The original pore space is widened and the pore fissures are connected (Fig. 13). The pore-crack system in the rock body is often attached and filled by minerals, the more minerals attached in the larger volume of pore-cracks, the greater the thickness of mineral attachment, and the higher the increase in permeability after dissolution [55]; and CO_2-water-rock coupling can also form new mineral crystals and precipitate and accumulate on the dissolution surface of the rock body (Fig. 16), which reduces the permeability of the rock body, and, in addition, some of the dissolution of the carbonate cement, which makes a large number of clay particles into the microscopic pore and fracture structure of the rock mass, and the expansion of clay minerals leads to the reduction of the flow of fracturing fluid in the pore and fracture [56]. It can be seen that the changes in

Table 4
The main interactions between sandstone samples and chemical solutions [33,53,54].

Reactive minerals	Chemical reaction equations
$KAlSi_3O_8$	$2KAlSi_3O_8 + 2H^+ + 9H_2O \rightarrow 2K^+ + Al_2Si_2O_5(OH)_4 \downarrow + 4SiO_2 \downarrow$ (8)
$NaAlSi_3O_8$	$2NaAlSi_3O_8 + 2H^+ + 9H_2O \rightarrow 2Na^+ + Al_2Si_2O_5(OH)_4 \downarrow + 4SiO_2 \downarrow$ (9)
$CaAl_2Si_2O_8$	$CaAl_2Si_2O_8 + 2H^+ + H_2O \rightarrow Ca^{2+} + Al_2Si_2O_5(OH)_4 \downarrow$ (10)
$Al_2Si_2O_5(OH)_4$	$Al_2Si_2O_5(OH)_4 + 2CO_3^{2-} + 2Na + 2H^+ \rightarrow 2NaAl(OH)_2CO_3 \downarrow + 2SiO_2 \downarrow + H_2O$ (11)
$CaMg(CO_3)_2$	$CaMg(CO_3)_2 + 2H^+ \rightarrow Ca^{2+} + Mg^{2+} + 2HCO_3^-$ (12)
$K_{0.6}Mg_{0.25}Al_{1.8}[Al_{0.5}Si_{0.35}O_{10}](OH)_2$	$K_{0.6}Mg_{0.25}Al_{1.8}[Al_{0.5}Si_{0.35}O_{10}](OH)_2 + 1.1H^+ + 3.15H_2O \rightarrow 0.6K^+ + 0.25Mg^{2+} + 1.15Al_2Si_2O_5(OH)_4 \downarrow + 1.2H_4SiO_4$ (13)
$Mg_{2.5}Fe_{2.5}Al_2Si_3O_{10}(OH)_8$	$Mg_{2.5}Fe_{2.5}Al_2Si_3O_{10}(OH)_8 + 10H^+ \rightarrow Al_2Si_2O_5(OH)_4 \downarrow + H_4SiO_4 + 2.5Mg^{2+} + 2.5Fe^{2+} + 5H_2O$ (14)

porosity and permeability are under the dual control of the erosion, dissolution and precipitation effects of the mineral components of the rock mass and the CO_2-coupled fracturing fluid, and the CO_2-water-rock coupling in this study has a greater erosion than precipitation effect on the sandstone samples as a whole, which in turn affects the mechanical strength of the rock mass to a certain extent. However, how to control the balance of dissolution and precipitation of sandstone minerals by controlling the chemical composition of the coupled fracturing fluid needs further study.

The CO_2 coupled fracturing fluid system has both chemical and physical effects on the rock mass. On the one hand, the physical effect is mainly manifested in the strong wetting ability of the coupling fracturing fluid to the rock body. Due to the injection of trace CO_2, the surface tension of the coupling fracturing fluid and its contact angle with the surface of the rock body are reduced, which enhances the wetting ability to the rock body, and the fracturing fluid not only penetrates along the fissures and structural surfaces of the rock body under the action of a certain injection pressure, but also enhances the penetration ability to the microporous fissures of the rock body, which makes it easier to penetrate the defective parts of the rock matrix. penetrate the defective parts in the rock matrix; on the other hand, with the continuous penetration of the CO_2-coupled fracturing fluid, the connectivity and friction between the mineral particles are reduced, coupled with the increase of pore pressure, the fracturing fluid produces an expansion effect within the pore cracks between the mineral particles, which results in the expansion of the volume of the pore cracks and the further extension of the pore cracks and at the same time, induces the generation of new pore cracks [57].

From the perspective of macroscopic damage, according to the Mohr-Coulomb strength theory, it is known that:

$$\tau = c + \sigma \tan \phi \tag{15}$$

Under the action of pore water pressure, the effective stress of the rock mass, at this time the strength of the rock mass is:

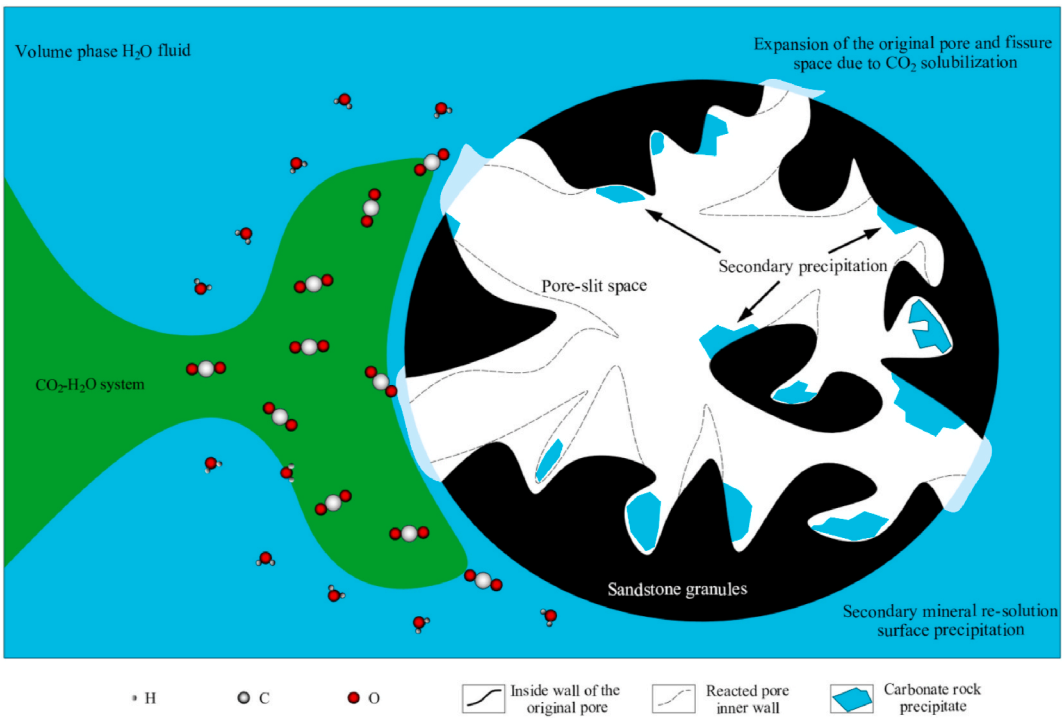

Fig. 16. Microporous structure evolution of shale during CO_2-water reaction process.

$$\tau = \sigma \tan \phi + (C - aP \tan \phi) \tag{16}$$

where a is the equivalent pore pressure coefficient, related to the degree of pore and fissure development of the rock body, the size of 0–1; P is the water pressure inside the pore and fissure, MPa; ϕ for the internal friction angle of the rock body, °; C is the cohesive force of the rock body, MPa.

According to previous studies, the compressive strength of the rock mass after water influence is [58]:

$$\sigma_w = \sigma_c - \frac{2aP \sin \phi}{1 - \sin \phi} \tag{17}$$

Equation (17) is the Mohr-Coulomb strength criterion under the action of pore water pressure, it can be seen that the cohesion of the rock body under the action of pore water pressure decreases $aP\tan\phi$,compressive strength decreases $\frac{2aP \sin \phi}{1-\sin \phi}$. From the above, it can be seen that CO_2-coupled fracturing fluids change the internal structure of the sandstone, the porosity, permeability, and wettability are enhanced, and the distribution range and flow ability of fracturing fluids in the rock body are increased. Compared with water, the CO_2-coupled fracturing fluid induced greater pore pressure in the rock mass, and the decrease in cohesion and compressive strength was greater, which was more likely to cause damage to the rock mass.

The chemical damage to the rock mass caused by the CO_2-coupled fracturing fluid reduces the mechanical strength of the rock mass, the minerals and plugs inside the microstructure of the rock mass are dissolved and eroded, a large number of cavities are increased in the vicinity of the walls of the fracturing boreholes and in the internal pores and cracks in the rock mass, and the degree of stress concentration is enhanced, and the pores and cracks under the action of the peripheral pressure undergo expansion, penetration and further expansion, and the porosity becomes larger, and the strength of the rock mass is reduced, and the permeability is enhanced. At the same time, due to the action of fracturing, the circulation and connection of fracturing fluid inside the rock mass and its pore and fracture structure were enhanced, and the range of acid corrosion inside the rock mass was further increased, which promoted the chemical damage to the rock mass, thus forming a CO_2-water-rock coupled chemical-mechanical damage cycle, and ultimately weakening the strength of the rock mass.

5. Conclusions

(1) Compared with the natural rock samples, the tensile strength and peak energy rate of each rock sample after CO_2-water-rock coupling are significantly reduced. The coupling temperature, pore pressure, fracturing fluid volume fraction and reaction time all have significant effects on the weakening degree of rock samples. The lower the coupling temperature, the higher the pore pressure, the higher the volume fraction of CO_2-coupled fracturing fluid, and the longer the coupling time, the greater the decrease in tensile strength. Under the conditions of reaction temperature of 25 °C, pore pressure of 7 MPa, and 8 % CO_2 action for 10.0h, the compressive strength of siltstone, fine-grained sandstone and coarse-grained sandstone decreased by 57.21 %, 53.73 % and 47.65 %, respectively.

(2) The coupling fracturing fluid penetrated into the internal pore and fracture structure of the specimen and had chemical reaction, the minerals in the pores were dissolved, and the pore and fracture volume fraction and fractal dimension increased to different degrees, while the mineral volume fraction and fractal dimension decreased.

(3) With the increase of coupling time, the damage pattern of sandstone samples after CO_2-water-rock coupling is affected by both chemical damage and mechanical damage, and the acid-rock reaction leads to the dissolution of minerals in the rock body and the development of fracture sprouting, while the unpressurized action further extends the pore and fracture and penetrates through the pore space, which further weakened the strength of the rock body. The degree of mineral dissolution and dissolution was greatest when the coupled fracturing fluid was CW-8. This study verifies the potential of CO_2-water-rock coupling to weaken sandstone and provides a theoretical reference for hard sandstone transformation.

Data availability

Data will be made available on request.

CRediT authorship contribution statement

Hongjian Li: Writing – review & editing, Writing – original draft, Visualization, Validation, Software, Investigation, Formal analysis, Data curation. **Guangzhe Deng:** Conceptualization.

Declaration of competing interest

The authors declare that they have no known competing financial interests or personal relationships that could have appeared to influence the work reported in this paper.

Acknowledgments

This work was supported by the Natural Science Foundation of Shaanxi Province, China (Grant Nos. 2019JLP09) and the Key Field Science and Technology Research Program of Xinjiang Production and Construction Corps (2019AB012), Xinjiang Production and Construction Corps key areas of science and technology research program funded projects (2019AB012). The authors also thank the anonymous reviewers for their helpful comments and suggestions.

Appendix B. Supplementary data

Supplementary data to this article can be found online at.

References

[1] Y. Ji, J. Fu, Y. Lu, et al., Three-dimensional-based global drought projection under global warming tendency, Atmos. Res. 291 (2023) 106812.
[2] J. Chen, et al., Impacts of climate warming on global floods and their implication to current flood defense standards, J. Hydrol. 618 (2023) 129236.
[3] C.E. Richards, H.L. Gauch, J.M. Allwood, International risk of food insecurity and mass mortality in a runaway global warming scenario, Futures 150 (2023) 103173.
[4] Y. Wang, et al., Micro-macro evolution of mechanical behaviors of thermally damaged rock: a state-of-the-art review, J. Rock Mech. Geotech. Eng 16 (7) (2024) 2833–2853.
[5] H. He, et al., Employing novel N-doped graphene quantum dots to improve chloride binding of cement, Construct. Build. Mater. 401 (2023) 132944.
[6] C. Liu, et al., The role of TBM asymmetric tail-grouting on surface settlement in coarse-grained soils of urban area: field tests and FEA modelling, Tunn. Undergr. Space Technol. 111 (2021) 103857.
[7] Y. Shen, N. Li, A. Hasnaoui, BRICS carbon neutrality target: measuring the impact of electricity production from renewable energy sources and globalization, J. Environ. Manag. 298 (2021) 113460.
[8] B. Xu, et al., Impacts of regional emission reduction and global climate change on air quality and temperature to attain carbon neutrality in China, Atmos. Res. 279 (2022) 106384.
[9] Saleem Raza, et al., Advances in technology and utilization of natural resources for achieving carbon neutrality and a sustainable solution to neutral environment, Environ. Res. 220 (2023) 115135.
[10] C. Zou, et al., Progress, challenge and significance of building a carbon industry system in the context of carbon neutrality strategy, Petrol. Explor. Dev. 50 (1) (2023) 210–228.
[11] H. He, et al., Exploring green and efficient zero-dimensional carbon-based inhibitors for carbon steel: from performance to mechanism, Construct. Build. Mater. 411 (2024) 134334.
[12] B. Bai, et al., Coupled thermo-hydro-mechanical mechanism in view of the soil particle rearrangement of granular thermodynamics, Comput. Geotech. 137 (2021) 104272.
[13] W. Liu, et al., Variable parameter creep model based on the separation of viscoelastic and viscoplastic deformations, Rock Mech. Rock Eng. 56 (6) (2023) 4629–4645.
[14] Z. Xu, et al., Characteristics of source rocks and genetic origins of natural gas in deep formations, Gudian Depression, Songliao Basin, NE China, ACS Earth Space Chem. 6 (7) (2022) 1750–1771.
[15] E.-M. Charalampidou, et al., Impact of CO_2-induced geochemical reactions on the mechanical integrity of carbonate rocks, Energy Proc. 114 (2017) 3150–3156.
[16] B. Yang, et al., Fundamental study and utilization on supercritical CO_2 fracturing developing unconventional resources: current status, challenge and future perspectives, Petrol. Sci. 19 (6) (2022) 2757–2780.
[17] Z. Shang, et al., The effect of leakage characteristics of liquid CO_2 phase transition on fracturing coal seam: applications for enhancing coalbed methane recovery, Fuel 308 (2022) 122044.
[18] Y. Jin, et al., Stress relaxation behaviour of marble under cyclic weak disturbance and confining pressures, Measurement 182 (2021) 109777.
[19] C. Ren, et al., A plastic strain-induced damage model of porous rock suitable for different stress paths, Rock Mech. Rock Eng. 55 (4) (2022) 1887–1906.
[20] X. Wang, et al., The influence of basalt fiber on the mechanical performance of concrete-filled steel tube short columns under axial compression, Frontiers in Materials 10 (2024) 1332269.
[21] K. Yang, et al., Chemical-mechanical coupling effects on the permeability of shale subjected to supercritical CO_2-water exposure, Energy 248 (2022) 123591.
[22] B. Elisenda, J.P. Kaszuba, S.J.T. Hangx, Assessing chemo-mechanical behavior induced by CO_2-water-rock interactions in clay-rich fault gouges, Procedia Earth and Planetary Science 17 (2017) 292–295.
[23] R. Prakash, et al., Chemical reactions of carbonate-rich mudstones with aqueous CO_2 and their impacts on rock's local microstructural and chemo-mechanical properties, J. Nat. Gas Sci. Eng. 103 (2022) 104587.
[24] D.S. Eyinla, et al., A comprehensive review of the potential of rock properties alteration during CO_2 injection for EOR and storage, Fuel 353 (2023) 129219.
[25] E. Berrezueta, et al., Laboratory studies on CO_2-brine-rock interaction: an analysis of research trends and current knowledge, Int. J. Greenh. Gas Control 123 (2023) 103842.
[26] J.K. Pearce, et al., Mineralogical controls on porosity and water chemistry during O_2-SO_2-CO_2 reaction of CO_2 storage reservoir and cap-rock core, Appl. Geochem. 75 (2016) 152–168.
[27] A. Al-Yaseri, et al., Rock-wettability impact on CO_2-carbonate rock interaction and the attendant effects on CO_2Storage in carbonate reservoirs, J. Nat. Gas Sci. Eng. 104 (2022) 104664.
[28] T. Yu, et al., Synergistic effects of CO_2 density and salinity on the wetting behavior of formation water on sandstone surfaces: molecular dynamics simulation, J. Nat. Gas Sci. Eng. 105 (2022) 104714.
[29] J. Geng, et al., Development and application of triaxial seepage test system for gas-water two-phase in coal rock, Energy 277 (2023) 127439.
[30] R. Azin, et al., Experimental study of CO_2–saline aquifer-carbonate rock interaction during CO_2 sequestration, Procedia Earth and Planetary Science 15 (2015) 413–420.
[31] Q. An, et al., Static and dynamic alteration effect of SC-CO_2 on rock pore evolution under different temperature and pressure: a comparative study, J. Nat. Gas Sci. Eng. 107 (2022) 104780.
[32] N. Li, et al., Investigation into shale softening induced by water/CO_2-rock interaction, Int. J. Rock Mech. Min. Sci. 161 (2023) 105299.
[33] Q. Niu, et al., The chemical damage of sandstone after sulfuric acid-rock reactions with different duration times and its influence on the impact mechanical behaviour, Heliyon 9 (2023) e22346.
[34] L. Yang, et al., Application of nano-scratch technology to identify continental shale mineral composition and distribution length of bedding interfacial transition zone-A case study of Cretaceous Qingshankou formation in Gulong Depression, Songliao Basin, NE China, Geoenergy Science and Engineering 234 (2024) 212674.

[35] J. Li, et al., Study on the shear mechanics of gas hydrate-bearing sand-well interface with different roughness and dissociation, Bull. Eng. Geol. Environ. 82 (11) (2023) 404.
[36] C. Ren, et al., Cyclic constitutive equations of rock with coupled damage induced by compaction and cracking, Int. J. Min. Sci. Technol. 32 (5) (2022) 1153–1165.
[37] T. Yang, et al., Five-DOF nonlinear tribo-dynamic analysis for coupled bearings during start-up, Int. J. Mech. Sci. 269 (2024) 109068.
[38] Dongxing Tang, et al., On the nonlinear time-varying mixed lubrication for coupled spiral microgroove water-lubricated bearings with mass conservation cavitation, Tribol. Int. (2024) 109381.
[39] F. Yu, G. Deng, The thermodynamic change laws of CO_2-coupled ractured rock, Appl. Sci. 14 (12) (2024) 5122.
[40] R. Zheng, et al., Experimental study on the effect of carbon dioxide fracturing fluids on the physical properties of coals, Sci. Technol. Eng. 23 (36) (2023) 15440–15447.
[41] Y. Zou, Y. Li, S. Li, Effects of CO_2 front injection on fracture morphology and rock physical properties in shale fracturing, Nat. Gas. Ind. 41 (10) (2021) 83–94.
[42] Y. Fan, et al., Experimental study of the influences of different factors on the acid-rock reaction rate of carbonate rocks, J. Energy Storage 63 (2023) 107064.
[43] Q. An, et al., Experiment on no-flow and flow CO_2-water–rock interaction: a kinetics calculation method for rock pore evolution, Chem. Eng. J. 464 (2023) 142754.
[44] C. Zhao, et al., Investigation on the mechanical behavior, permeability and failure modes of limestone rock under stress-seepage coupling, Eng. Fail. Anal. 140 (2022) 106544.
[45] G. Wang, et al., Experimental study on microstructural changes and evolution laws of sandstone under different temperature effects, Journal of Rock Mechanics and Engineering 43 (3) (2024) 600–610.
[46] J. Feng, et al., Macro-micro features of Jurassic sandstones in northern Shaanxi and their water-richness response mechanism, Coal Sci. Technol. 51 (7) (2023) 167–178.
[47] X. Sun, et al., Quantitative characterization of water absorption pore structure evolution in sandstone based on nitrogen adsorption and mercury intrusion, J. Cent. S. Univ. 31 (1) (2024) 182–195.
[48] B. Huang, et al., The efect of overlying rock fracture and stress path evolution in steeply dipping and large mining height stope, Geomech. Geophys. Geo-energ. Geo-resour 10 (1) (2024) 1–19.
[49] Y. Zhang, et al., CT-based quantitative characterization of three-dimensional rock fissures and microscopic study of their propagation and evolution, Geomechanics 42 (10) (2021) 2659–2671.
[50] Chengzu He, Hua Mingqi, Fractal geometry description of reservoir pore structure, Petroleum and natural gas geology 1 (1998) 17–25.
[51] V. Brotóns, et al., Temperature influence on the physical and mechanical properties of a porous rock: san Julian's calcarenite, Eng. Geol. 167 (2013) 117–127.
[52] M.A. Rajabzadeh, et al., Effects of rock classes and porosity on the relation between uniaxial compressive strength and some rock properties for carbonate rocks, Rock Mech. Rock Eng. 45 (2012) 113–122.
[53] S. Li, et al., Effect of acid-temperature-pressure on the damage characteristics of sandstone, Int. J. Rock Mech. Min. Sci. 122 (2019) 104079.
[54] S. Li, et al., Experimental study on physicomechanical properties of sandstone under acidic environment, Adv. Civ. Eng. 2018 (2018).
[55] Kam Ng, J. Carlos Santamarina, Mechanical and hydraulic properties of carbonate rock: the critical role of porosity, J. Rock Mech. Geotech. Eng. 15 (4) (2023) 814–825.
[56] J. Kaszuba, B. Yardley, M. Andreani, Experimental perspectives of mineral dissolution and precipitation due to carbon dioxide-water-rock interactions, Rev. Mineral. Geochem. 77 (1) (2013) 153–188.
[57] B. Deng, et al., Feature of fractures induced by hydrofracturing treatment using water and L-CO_2 as fracturing fluids in laboratory experiments, Fuel 226 (2018) 35–46.
[58] B. Shu, J. Chen, H. Xue, et al., Experimental study of the change of pore structure and strength of granite after fluid-rock interaction in CO_2-EGS, Renew. Energy 220 (2024) 119635.